Optimisation of Stilling Basin Chute Blocks Using a Calibrated Multiphase RANS Model

D. Valero[1], R. García-Bartual[1] and J. Marco[1]
[1]Instituto Universitario de Investigación de Ingeniería del Agua y Medio Ambiente
Universitat Politècnica de València
Cno. de Vera s/n 46022 València
SPAIN
E-mail: davahue@upv.es

Abstract: *Interaction between chute blocks and highly aerated flows has been studied in this paper. For this purpose, a RANS model coupled with a calibrated turbulent air entrainment model, VOF method and RNG $k-\varepsilon$ turbulence model have been employed. This has allowed analysing the complex multiphase flows behaviour in an USBR type II stilling basin with variable chute block height. Furthermore, conducted simulations exhibit some similarities with flow patterns detected in previous B-jump, hydraulic jump and highly aerated flows experimental studies. Finally, it has been also possible to identify two different mechanisms involving the chute blocks effect upon the flow: turbulent rough wall jet and flow deflector. Turbulent wall jet mechanism takes place for lower values of the chute block height and helps to stabilise hydraulic jump for deficient tail water conditions while flow deflector has not shown to be a desirable mechanism in a stilling basin.*

Keywords: *stilling basins design, CFD, RNG $k-\varepsilon$, free surface, air entrainment, VOF.*

1. INTRODUCTION

Multiphase flows have got hydraulic researchers attention during the last two decades. Air entrained has become one of the main variables in the study of large spillways performance as it can prevent cavitation damage (Falvey, 1990; Kramer *et al*, 2006). However, high rates of air concentration can reduce water-solid friction (Wood, 1991), generating flow acceleration and increasing maximum velocities at the inlet of the stilling basin. Air entrained also produces a turbulence modulation inside the flow body producing different energy dissipation rates (Balachandar & Eaton, 2010). In addition, momentum differs from non-aerated flow since macroscopic density changes. Hence, multi-phase flows in hydraulic structures usually exhibit modified flow features in comparison to the counterpart only water flows as detected in previous experimental studies (Valero *et al*, 2014; Pfister & Hager, 2012).

Extensive experimental researches have been made to characterize aerated flows past hydraulic structures obtaining variables such as air concentration and velocity distribution (Chanson, 2013; Pfister & Hager, 2010; Bung, 2011; Pfister, 2008; Kramer *et al*, 2006; Hager, 1991). Frequently aerated spillways physical models are affected by scale effects, with Weber and Reynolds numbers being usually too low to adequately reproduce observed flows (Heller, 2011).

During recent years, important advances took place thanks to the emergence of the so-called Computational Multi-Phase Fluid Dynamics (Prosperetti & Tryggvason, 2007; Bombardelli, 2012), which arises as an efficient tool to simulate real flows in hydraulic structures. To the knowledge of the authors, few attempts have been made to reproduce highly aerated flows in hydraulic structures although these computational techniques allow 1:1 scale simulations, free of scale effects. However, 3D numerical simulations of supercritical spillway flows are time expensive and air water interfacial processes would need fine resolution meshes which require extensive computing. Nevertheless, some multiphase hydraulic numerical researches have been conducted in the last years (Meireles *et al*, 2014; Jha & Bombardelli, 2010; Ma *et al*, 2011a, 2011b).

RANS models, which require lower computational costs, are well suited for hydraulic problems despite its limitations (Carvalho *et al*, 2008). Similarly, the use of a sub-grid scale in air entrainment models can be useful to predict air entrained quantities within free surface cells. Then, flow behaviour can be more accurately assessed with a variable density formulation. However, lack of validation and

verification is still an issue pointed out by several researchers (Chanson, 2013; Chanson & Lubin, 2010). Thus, these numerical models new results should be carefully validated.

In this research, an USBR type II stilling basin performance is studied varying the chute blocks height. The basin elements which interact more with the highly aerated flow are precisely these chute blocks. Chute blocks bear some resemblance to baffle piers but their function is altogether different. Chute blocks at the upstream end of a basin tend to corrugate the jet, lifting a portion of it from the floor to create a greater number of energy dissipating eddies, resulting in a shorter length of jump than would be possible without them. These blocks also reduce the tendency of the jump to sweep off the apron at tail water elevations below conjugate depth (Peterka, 1984). Thus, they help stabilising the hydraulic jump. Despite the amount of studies carried out, only a reduced range of chute blocks heights have been analysed. In this research, chute blocks heights ranging from 1.0 to 10.7 h_w are studied analysing the resulting flow patterns which take place at the stilling basin and evaluating its role as a hydraulic jump stabiliser. The case for none chute blocks, corresponding with the sloping B-jump (Ohtsu, 1991; Kawagoshi & Hager, 1990), has also been studied which has resulted in good agreement with previous experimental data.

In order to reproduce properly the flow conditions at the inlet of the energy dissipation structure, FLOW-3D routine for turbulent air entrainment is used, coupled with variable density evaluation, Volume-of-Fluid (VOF) method and a drift-flux model which accounts for the effect of the air bubbles upon the carrier phase (i.e.: the water phase). The $k-\varepsilon$ RNG turbulence model is also employed. For the turbulent air entrainment model, calibrated values of the parameters have been used (Valero & García-Bartual, 2014). These values have been obtained in a calibration process involving over 200 prototype scale spillway flow simulations.

2. MATHEMATICAL MODEL

Reynolds Averaged Navier-Stokes equations (RANS) have been numerically solved (Pope, 2000) coupled with a RNG $k-\varepsilon$ turbulence model, being κ the turbulent kinetic energy and ε the turbulent dissipation rate, both modeled by their respective transport equations (Wilcox, 1998; Yakhot, 1992). VOF method (Hirt & Nichols, 1981; Meireles *et al*, 2014; Oertel & Bung, 2012; Carvalho *et al*, 2008) included in the FLOW-3D code has been used for free surface tracking. Turbulence and free surface models are essential for the correct assessment of the free surface profile and the turbulence quantities which are the input for the turbulent air entrainment model following introduced. FAVOR method for geometry representation (Hirt & Sicilian, 1985) and multi-block meshes have been employed to allow a correct representation of the hydraulic structure geometry and adequate refinement (Bombardelli *et al*, 2011). For advection numerical approximation, an explicit second order scheme with monotonicity preserving has been employed. More information about this method can be found in (Hirsch, 2007).

Turbulent air entrainment and drift-flux models are employed in order to reproduce high aerated flows behaviour. The air entrainment model is responsible for predicting entrainment of air pockets smaller than the finest cell resolution while drift-flux model adds the disperse phase effect upon the carrier phase. For this purpose, a drag component is added to the governing equations. Thus, coarser computational grids can be employed avoiding unaffordable, too costly simulations.

2.1. Air-water flow modelling

A turbulent air entrainment model is used for the estimation of air entrained volumes across the free surface. A characteristic size of turbulent eddies may be defined as follows:

$$L_T = C_\mu \sqrt{\frac{3}{2}} \frac{k^{3/2}}{\varepsilon} \tag{1}$$

With $C_\mu = 0.085$ as used for the RNG $k-\varepsilon$ turbulence model, which calculates k and ε in every step at every cell. L_T value varies depending on the chosen turbulence model, while k and ε quantities are

also affected by the air entrainment model with a buoyancy production term. Therefore, both models are implicitly coupled. This length scale is used to characterize turbulent surface disturbances.

According to (Hirt, 2003), the energy density associated with a disturbed fluid element raised over the free surface to a height L_T, can be expressed considering two components (gravity and surface tension):

$$P_d = \rho g_n L_T + \frac{\sigma}{L_T} \tag{2}$$

Where ρ is the macroscopic fluid density, g_n is the gravity component normal to the free surface and σ is the liquid-gas surface tension. Thus P_d represents a surface stabilising force, while P_t (turbulent kinetic energy per unit volume) represents the perturbing component that makes the flow unstable:

$$P_t = \rho k \tag{3}$$

Air entrainment occurs when $P_t > P_d$. The corresponding air entrained volume (per unit time) can be computed as:

$$\delta V = C_{air} A_s \sqrt{2 \frac{P_t - P_d}{\rho}} \tag{4}$$

Where $C_{air} = 0.525$ is a parameter calibrated using prototype experimental data (Valero & García-Bartual, 2014) and A_s is the free surface area at each cell, which depends strongly on the free surface model. This air volume δV is taken into account affecting macroscopic density of the mixture and producing bulking of the flow. This macroscopic density is computed as:

$$\rho = (1 - C_{ent})\rho_w + C_{ent}\rho_a \tag{5}$$

Where C_{ent} is the computed entrained air at every cell, ρ_w the water density and ρ_a the air density. It is also assumed that air entrained form bubbles of an only characteristic diameter. Thus, bubbles produce a drag force upon the carrier phase which opposes to the water movement. It is computed a relative velocity between both phases and used a so called drift-flux model (Brethour & Hirt, 2009). For this purpose, a bubble diameter of 0.005 m has been employed in all simulations.

Additionally, entrapped air occurs as high velocity flows drag some large air volumes due to its free surface roughness (Wilhelms & Gulliver, 2005). Despite it is not explicitly computed at the described model, entrapped air is represented by the voids of the free surface modelling which is a consequence of the turbulence induced surface roughness. Therein, this is representing a lack of momentum but not a shear stress over the free surface as simulations are carried out with a 1 fluid approach (Prosperetti & Tryggvason, 2007); hence not solving the air phase. Averaging over time, mean total conveyed air can be expressed as the sum of mean entrained air ($\bar{C}_{ent}$) and mean entrapped air ($\bar{C}_{rough}$):

$$\bar{C}_{total} = \bar{C}_{ent} + \bar{C}_{rough} \tag{6}$$

For a flow section, it can be denoted a transition depth y_t which separates the air dispersed phase from the water dispersed phase; and consequently the predominant air entrained region from the air entrapped region. It is also usually defined an equivalent clean water depth (Wood, 1991), which is the only water part of the two-phase flow depth:

$$h_w = \int_{y=0}^{y=y_{95}} (1 - \bar{C}_{total}) dy \tag{7}$$

With y_{95} the depth where $\bar{C}_{total} = 0.95$. All these quantities are outlined in figure 1.

3. MODEL SETUP

The modelled geometry consists of two parts: an ogee spillway and an USBR type II stilling basin. The spillway has been designed as described in (Peterka, 1984) for a design head $H_d = 1$ m, which gives

as a result a specific flow rate of 2.18 m^2/s. Spillway height is set to $H = 20$ m. The spillway slope is 0.75H:1V, (53.13 degrees slope). Stilling basin is composed of chute blocks and an end sill. Most relevant geometry features are sketched in figure 1. Surface roughness of all the elements was set to 1 mm.

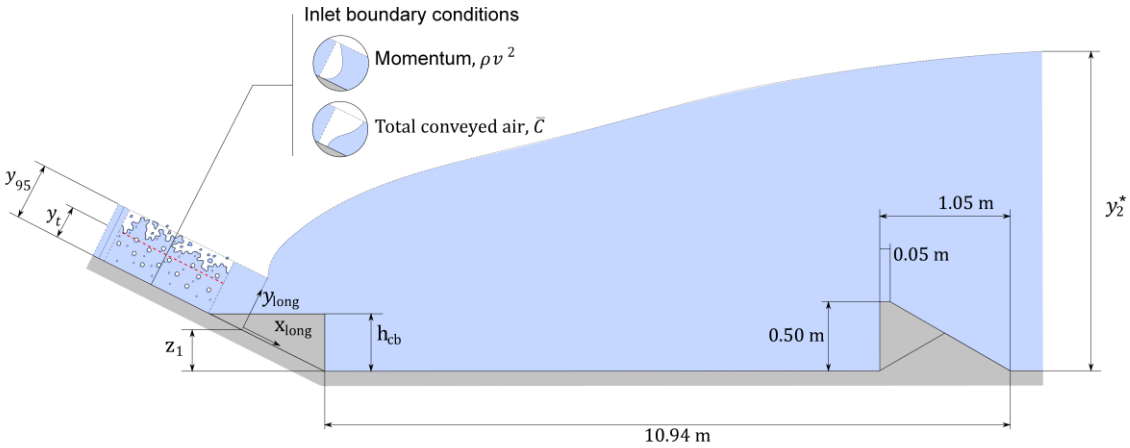

Figure 1. Stilling basin geometry and inlet boundary condtions.

According to (Peterka, 1984), the outlet velocity for this spillway is $v_1 = 15.4$ m/s, with a supercritical depth of $h_w = 0.141$ m, which gives a Froude number $F_{1,w} = v_1/\sqrt{g\, h_w} = 13.2$. The conjugate depth is calculated obtaining $y_2 = 2.54$ m. Different tail water depths ($y_2{}^*$) are employed in the simulations. The value of the stilling basin length and the end sill dimensions are fixed whereas the chute blocks height h_{cb} remains variable as its optimum value is the aim of this study. The chute blocks heights studied are: $h_{cb} = 0$, $1.0\, h_w$, $3.1 h_w$, $7.1\, h_w$ and $10.7\, h_w$.

In order to reproduce a reliable inlet conditions, the entire spillway and a part of the reservoir is simulated with a 2D mesh. It has been used the same multi-block meshes with cubic cells for all the conducted simulations. For the spillway, the employed cell size was set to $\Delta x = 0.04\, m$, which has been shown to be fine enough to reproduce these supercritical flow main features (Valero & García-Bartual, 2014). For the rest of the domain, three 3D meshes with cubic cells with size cell values of 0.04 m, 0.08 m and 0.16 m have been used, arising 3.8 millions of total cells. Mesh characteristics are shown in table 1.

Table 1. Mesh characteristics.

	type	Δx (m)	No. Cells	large (m)	width (m)	height (m)	Region
Mesh 1	2D	0.04	262500	21.0	5.0	20.0	Spillway and reservoir
Mesh 2	3D	0.04	2340000	4.8	5.0	6.0	Chute blocks and impact
Mesh 3	3D	0.08	1124240	10.2	5.0	7.36	Stilling basin
Mesh 4	3D	0.16	84000	12.0	5.0	5.6	Downstream flow condition

Moreover, 2 different scenarios have been modelled for an improved evaluation of the effect of the chute blocks height upon the flow. The first one, consists of a statistically steady state with the recommended tail water level ($y_2{}^*/y_2 = 1.05$); and the second one is a transient simulation with a decreasing tail water depth. Thereby, it is not only studied the dissipation properties of the basin but also the stabilising effect of the chute blocks.

For the stationary scenario, a first simulation with $h_{cb} = 1.0\, h_w$ was carried out for 60 seconds, showing statistically stationary conditions after 25 seconds, both for volume of fluid in the domain and turbulent kinetic energy. The other simulations were conducted for 30 seconds, obtaining similar curves for volume of fluid and turbulent kinetic energy.

For the transient case, all simulations were conducted for 30 seconds employing the stationary water profile of prior simulations as the initial solution. Then, simulation advances in time decreasing

exponentially the tail water depth at the downstream boundary condition, forcing thereby the hydraulic jump to escape from chute blocks region for all simulations.

4. RESULTS

In order to avoid instantaneous flow oscillations over the extracted profiles, the simulations solutions for steady scenario have been averaged over the last 5 seconds. This time scale has shown to be superior to the oscillation period of the total energy and the volume of fluid taking place in the simulation domain. Hence, it has been obtained the mean velocity field, mean fluid fraction and mean air concentration. This allows computing mean entrapped air concentration as the mean void fraction (i.e.: the lack of fluid fraction at every cell).

Figure 2 shows the mean total conveyed, entrained and entrapped air concentration profiles at the inlet section for the simulation with $h_{cb} = 1.0\ h_w$. It has also been plotted an experimentally based air profile (Chanson, 1993). As can be observed, it is similar to the numerically obtained profiles. Although not plotted herein, other inlet air concentration profiles were also compared, with similar results.

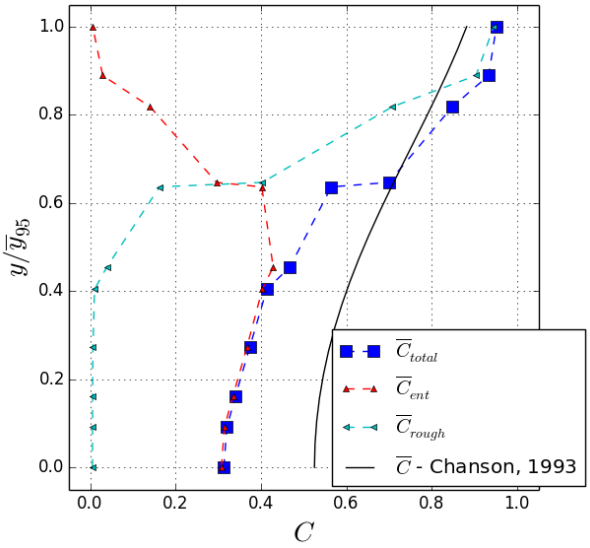

Figure 2. Air concentration profiles at the stilling basin inlet section.

It has been observed that air entrained is predominant in the region close to the bottom of the spillway while air entrapped only affects the surface region. It is also shown in figure 2 that this transition (y_t from figure 1) takes place at the first cell above $C = 0.50$, which has been identified experimentally as a transition value for entrained and entrapped air (Pfister, 2008). Free surface intermittency after the inception point has been also observed, although it was not compared to theoretical values (Wilhelms & Gulliver, 2005).

Regarding representative values for air concentration, experimentally based formulations give for the bottom concentration a value of $\bar{C}_0 = 0.52$ and for the mean air concentration, $\bar{C}_{total} = 0.63$ (Hager, 1991). After numerical simulations, the resulting values are respectively $\bar{C}_0 = 0.31$ and $\bar{C}_{total} = 0.57$, which represents an error of 40 % for $\bar{C}_0$, but only a 10 % for $\bar{C}_{total}$. The main source of error seems to be at the entrained air computed value. Despite the significant difference occurring in the bottom, authors believe that air concentration profile is good enough to represent the inlet boundary condition of this study. Improving the result for the bottom concentration would require a modification of the actual air entrainment model. However, this value is of critical importance since it is the one which really prevents spillway surface from cavitation.

The equivalent water depth h_w ranges between 0.1252 m and 0.1431 m in the conducted simulations, with a mean value of 0.135 m. It is therefore in good agreement with the calculated depth ($h_w = 0.141$ m) employing the USBR abacus for actual and theoretical velocity correction (Peterka, 1984).

4.1. Statistically steady scenario

Given the analogy of the conducted simulations to the B-jump in sloping channels (Peterka, 1984; Ohtsu & Yasuda, 1991), where the jump is formed partly in the sloping portion and partly in the horizontal channel portion (without chute blocks); submergence parameter has been calculated for all the cases as (Kawagoshi & Hager, 1990):

$$E = \frac{{y_2}^* - z_1}{{y_2}^*} \tag{8}$$

Where z_1 is the height of the toe position measured as shown in figure 1. B-jumps are described by $0 < E < 1$, whereas $E = 1$ is the upper limit and holds for A-jump, the most efficient case. This quantity has been measured for the averaged solution over the last 5 seconds of the simulation. The hydraulic jump efficiency enhances as the submergence parameter increases. The position of the toe is selected contemplating the mean fluid fraction iso-surface with value 0.5. The values of the submergence parameter for all the simulations are shown in the Table 2.

Table 2. Toe position and submergence parameter values.

h_{cb}	$z_1\ (m)$	${y_2}^*\ (m)$	E
0	2.558	2.672	0.043
$1h_w$	2.277	2.672	0.148
$3.1h_w$	2.533	2.672	0.052
$7.1h_w$	2.696	2.672	-0.009
$10.7h_w$	2.787	2.672	-0.043

It should be noticed that lower values of h_{cb} lead to better submergences, while large values lead to negative submergences otherwise. For all the cases, the submergences were expected to be close to zero as the downstream energy is high enough, as shown in the previously mentioned experimental studies.

Regarding the flow structure within the stilling basin, maximum velocity decay along the stilling basin has been compared to classic turbulent wall jet (Rajaratnam, 1976) and classic hydraulic jump (Chanson, 2000), which better represent the main flow patterns observed within this energy dissipation structures (Kawagoshi & Hager, 1990; Ohtsu & Yasuda, 1991).

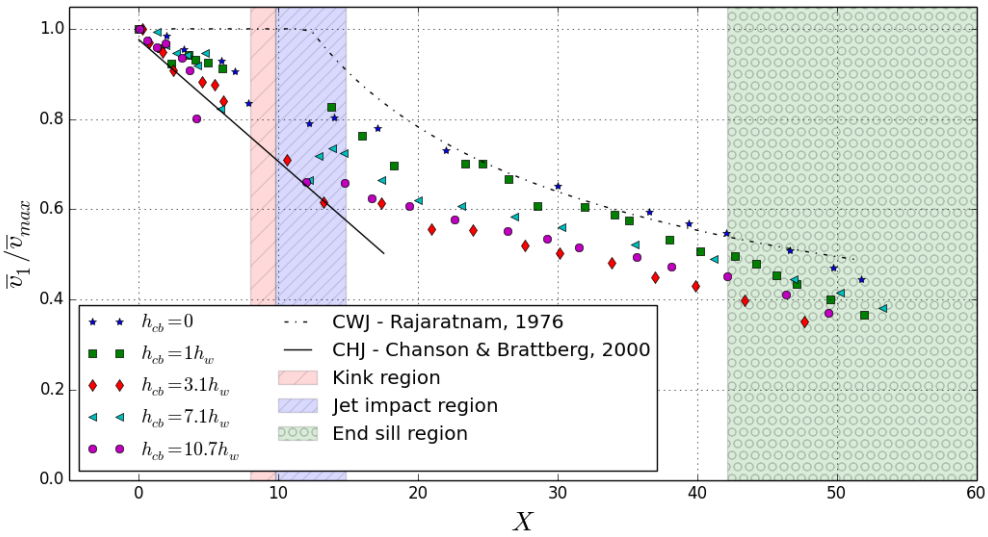

Figure 3. Maximum velocity decay starting at the toe position. Comparison with the classic turbulent wall jet (Rajaratnam, 1976) and the Classic Hydraulic Jump data (Chanson, 2000).

It can be observed the result for all the simulations in figure 3. It has been employed a normalized longitudinal coordinate $X = x_{long}/\bar{y}_{95}$; being x_{long} the longitudinal distance starting at the toe position (see figure 1).

The maximum velocity decay holds between the classic hydraulic jump and the classic wall jet, remaining more similar to the classic wall jet as noticed by (Kawagoshi & Hager, 1990) for sloping jumps with low submergence parameter. Acceleration zone after the junction, due to streamline curvatures, can also be observed as pointed out by (Ohtsu & Yasuda, 1991).

The most similar case to the turbulent wall jet occurs for $h_{cb} = 0$. Thus, the larger chute blocks show a velocity decay closer to the hydraulic jump curve. Higher values of h_{cb} divide the inlet flow into parallel jets, ones impacting at the chute blocks and others at the junction, and then quickly colliding after the impact region altogether. Hence, jets colliding over the chute blocks raise the water level diminishing the submergence parameter and thus the jump efficiency.

Different performance is observed for the case $h_{cb} = 1.0\, h_w$, where the acceleration zone is skipped while the decay tendency is closer to that of a rough wall turbulent jet (Rajaratnam, 1976). Results suggest that small chute blocks induce some turbulence which helps to dissipate energy along the stilling basin as a continuum.

4.2. Transient scenario

The aim of the transient analysis is to assess the energy dissipation structure performance under deficient downstream conditions with a reasonable computational cost. Thus, the tail water level is decreased exponentially during 30 seconds reaching about the 25 % of the previously calculated conjugate depth. As a result, the hydraulic jump is forced to sweep off the chute blocks region for all the cases. There, hydraulic jump becomes sill controlled and chute blocks have a negligible effect upon the hydraulic jump.

Result of the transient analysis is shown in figure 4. It has been observed that any chute block size benefits the stability of the stilling basin except for the highest value studied ($h_{cb} = 10.7\, h_w$). The cases for medium values of h_{cb} are very similar. However, $h_{cb} = 1.0\, h_w$ holds a higher value of the submergence parameter along time, providing a higher efficiency for a wider range of tail water conditions.

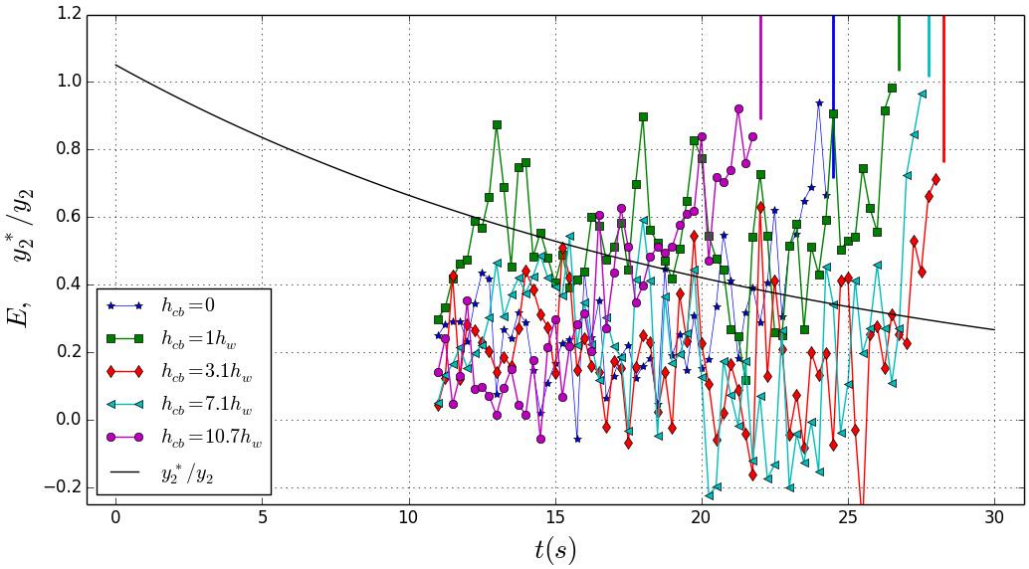

Figure 4. Transient evolution of the submergence parameter and the tail water boundary condition. Solid vertical wider lines mark off the sweep off time value.

5. CONCLUSIONS

In this research, it has been analysed the complex multiphase flows taking place within an USBR type II stilling basin with varying chute blocks height. For this purpose, a RANS model coupled with a calibrated turbulent air entrainment model, a VOF method and the RNG $k-\varepsilon$ turbulence model have been employed.

Conducted simulations show good agreement with the experimental data for both the naturally aerated flow in the spillway and the sloping B-jump (which corresponds to the case $h_{cb}=0$). Additionally, it has been observed that the air entrained and entrapped regions, as well as the transition point, are well reproduced despite the significant differences in the bottom concentration. Moreover, acceleration regions and turbulent wall jet behavior has been detected for the velocity decay as reported by previous experimental researchers. Finally, it was possible to clearly identify two different flow patterns depending on the h_{cb}/h_w ratio, allowing evaluation of the change in the hydraulic jump structure and the stabilising effect of the chute blocks height for deficient downstream conditions.

More research is needed in the lines of air entrainment sub-scale models performance. Collision terms for highly aerated regions, turbulent diffusion, turbulence modulation and a polydisperse bubble size may should improve air concentration profiles predictions and its effect upon the main flow. More advanced turbulence models for free surface turbulence representation can also help to take into account the air effect in the 1 fluid approach formulation. The large amount of available experimental data about aerated flows characteristics could yield a better validation of these sub-scale models.

6. ACKNOWLEDGMENTS

The research described in this paper has been carried out under the research project “Natural and forced air entrainment in dam spillways and potential range of operation enlargement for hydraulic jump energy dissipators”, BIA2011-28756-C03-01, supported by the Spanish Ministry of Economy and Competitiveness and by ERDF funding of the European Union.

7. REFERENCES

Balachandar, S. and Eaton, J.K., (2010), *Turbulent Dispersed Multiphase Flow*. Annu. Rev. Fluid Mech, 2010, 42:111-33.

Bombardelli, F.A., Meireles, I. and Matos, J. (2011), *Laboratory measurements and multi-block numerical simulations of the mean flow and turbulence in the non-aerated skimming flow region of steep stepped spillways*. Environmental Fluid Mechanics, 11(3), 263-288.

Bombardelli, F. (2012), *Computational multi-phase fluid dynamics to address flows past hydraulic structures*. *4th IAHR Inernational Symposium on Hydraulic Structures*, February 9 – 11, 2012, Porto, Portugal. ISBN: 978-989-8509-01-7.

Brethour, J.M. and Hirt, C.W. (2009), *Drift Model for Two-Component Flows*. FSI-09-TN83Rev. FlowScience, Inc.

Bung, D.B. (2011), *Developing flow in skimming flow regime on embankment stepped spillways*. Journal of Hydraulic Research, 49(5), 639-648.

Carvalho, R.F., Lemos, C.M. and Ramos, C.M. (2008), *Numerical computation of the flow in hydraulic jump stilling basins*. Journal of Hydraulic Research, 46(6), 739-752.

Chanson, H., and Brattberg, T. (2000), *Experimental study of the air–water shear flow in a hydraulic jump*. International Journal of Multiphase Flow, 26(4), 583-607.

Chanson, H. and Lubin, P. (2010), *Verification and validation of a computational fluid dynamics (cfd) model for air entrainment at spillway aerators*. Can. J. Civil Eng. 37(1), 135-138.

Chanson, H. (2013), *Hydraulics of aerated flows: qui pro quo?.* Journal of Hydraulic Research, 51:3, 223-243.

Falvey, H.T. (1990), *Cavitation in chutes and spillways*. USBR Engineering Monograph, No. 42, Denver, CO.

Hager, W.H. (1991), *Uniform aerated chute flow*. Journal of Hydraulic Engineering, 117(4), 528-533.

Heller, V. (2011), *Scale effects in physical hydraulic engineering models*. Journal of Hydraulic Research, 49(3), 293-306.

Hirsch, C. (2007), *Numerical Computation of Internal and External Flows: The Fundamentals of Computational Fluid Dynamics: The Fundamentals of Computational Fluid Dynamics*. Butterworth-Heinemann.

Hirt, C.W. (2003), *Modeling Turbulent Entrainment of Air at a Free Surface*. FSI-03-TN61-R. Flow Science, Inc.

Hirt, C.W. and Nichols, B.D. (1981), *Volume of fluid (VOF) method for the dynamics of free boundaries*. Journal of Computational Physics, 39(1), 201-225.

Hirt, C.W. and Sicilian, J.M. (1985), *A porosity technique for the definition of obstacles in rectangular cell meshes*. In Proc. Fourth International Conf. Ship Hydro.

Jha, S.K. and Bombardelli, F.A. (2010), *Toward two-phase flow modeling of nondilute sediment transport in open channels*. Journal of Geophysical Research: Earth Surface (2003–2012), 115(F3).

Kawagoshi, N., and Hager, W.H. (1990), *B-jump in sloping channel, II.* Journal of Hydraulic Research, 28(4), 461-480.

Kramer, K., Hager, W.H. and Minor, H.E. (2006), *Development of air concentration on chute spillways*. Journal of Hydraulic Engineering, 132(9), 908-915.

Ma, J., Oberai, A.A., Drew, D.A., Lahey, R.T. and Hyman, M.C. (2011a), *A comprehensive sub-grid air entrainment model for RaNS modeling of free-surface bubbly flows*. The Journal of Computational Multiphase Flows, 3(1), 41-56.

Ma, J., Oberai, A.A., Lahey Jr, R.T. and Drew, D.A. (2011b), *Modeling air entrainment and transport in a hydraulic jump using two-fluid RANS and DES turbulence models*. Heat and mass transfer, 47(8), 911-919.

Meireles, I.C., Bombardelli, F.A. and Matos, J. (2014), *Air entrainment onset in skimming flows on steep stepped spillways: an analysis*. Journal of Hydraulic Research, Vol. 52, Iss. 3, 375-385.

Oertel, M. and Bung, D.B. (2012), *Initial stage of two-dimensional dam-break waves: Laboratory versus VOF*. Journal of Hydraulic Research, 50(1), 89-97.

Ohtsu, I. and Yasuda, Y. (1991), *Hydraulic jump in sloping channels*. Journal of Hydraulic Engineering, 117(7), 905-921.

Peterka, A.J. (1984), *Hydraulic design of spillways and energy dissipators*. A Water Resources Technical Publication, Engineering Monograph, (25).

Pfister, M. (2008), *Bubbles and waves description of self-aerated spillway flow*. Journal of Hydraulic Research, Vol. 46, Iss. 3, 420-423.

Pfister, M. and Hager, W.H. (2010), *Chute aerators. I: Air transport characteristics*. Journal of Hydraulic Engineering, 136(6), 352-359.

Pfister, M. and Hager, W.H. (2012), *Deflector-jets affected by pre-aerated approach flow*. Journal of Hydraulic Research, 50(2), 181-191.

Pope, SB. (2000), *Turbulent flows*. Cambridge university press.

Prosperetti, A. and Tryggvason, G. (2007), *Computational methods for multiphase flow*. Cambridge University Press.

Rajaratnam, N. (1976), *Turbulent jets*. Elsevier.

Valero, D. and García-Bartual, R. (2014), *Calibration of an air entrainment model for CFD spillway applications. SimHydro 2014: Modelling of rapid transitory flows*, June 11-13 2014, Sophia Antipolis.

Valero, D., Fullana O., García-Bartual, R., Andrés-Doménech, I, Vallés, F. and Marco, J. (2014), *Analytical formulation for the aerated hydraulic jump and physical modeling comparison. 3rd Europe IAHR Congress, Book of Proceedings*, April 14 – 18, 2014, Porto – Portugal.

Wilcox, D.C. (1998). *Turbulence modeling for CFD*. La Canada, CA: DCW industries.

Wilhelms, S.C. and Gulliver, J.S. (2005), *Bubbles and waves description of self-aerated spillway flow*. Journal of hydraulic research, 43(5), 522-531.

Wood, I.R. (1991), *Air entrainment in free-surface flows*. IAHR Hydraulic Design Manual No.4, Hydraulic Design Considerations, Balkema Publications, Rotterdam, The Netherlands.

Yakhot, V., Orszag, S.A., Thangam, S., Gatski, T.B. and Speziale, C.G. (1992), *Development of turbulence models for shear flows by a double expansion technique*. Physics of Fluids A: Fluid Dynamics, 4, 1510.